NATIONAL TRANSPORTATION SAFETY BOARD
Office of Research and Engineering
Materials Laboratory Division
Washington, D.C. 20594

July 8, 2022

MATERIALS LABORATORY FACTUAL REPORT Report No. 22-049

1. ACCIDENT INFORMATION

Place	:	Azusa, California
Date	:	March 19, 2022
Vehicle	:	Eurocopter AS3321L1, N950SG
NTSB No.	:	WPR22LA125
Investigator	:	Fabian Salazar, AS-WPR

2. COMPONENTS EXAMINED

Remnants of seat belt clips

3. DETAILS OF THE EXAMINATION

On March 19, 2022, about 1704 Pacific daylight time, a Eurocopter AS332L1 helicopter was substantially damaged when it was involved in an accident near, Azusa, CA. The two pilots and two passengers were seriously injured, and two passengers received minor injuries. According to the pilot in command, during the approach and about 5 feet above the ground, the helicopter contacted a tree, descended to the ground, and rolled over onto its left side. During the rollover sequence, the pilot's lap belt separated from the seat. Preliminary examination of the right pilot's seat revealed the two lap belt retention brackets fractured. The helicopter was recovered to a secure location for further examination.

Figure 1 and Figure 2 show the fractured seat belt clips, as received. The clips were labeled A and B prior to receipt, with the two fragments of the A clip labeled A1 and A2. There was only one fragment from the B clip received.

Both clips exhibited markings indicating the manufacturer: "AUTOFLUG". The A2 remnant had the marking, "AFG-40691". There was no such marking available on the B clip remnant, as the fractured bridge segment was not received.

The clasps on each clip were able to be actuated. There were circumferential wear patterns around the inside surfaces where the clasps enclosed. These worn areas were approximately 1/8 inch in thickness, as can be seen in Figure 1 for the B clip and Figure 2 for the A clip. There were no indications of gouges or cracks emanating from these areas.

Both clips had fractured near the corner of the bottom bridge near the two arms, as demonstrated in the figures. Closer views of the four fracture surfaces are shown in Figures 3 through 6.

Both arms with the riveted clasp connection fractured approximately 0.20 inches from the rivet. In each of these locations, the arm exhibited localized necking adjacent to the fracture surface (see Figures 1 and 2). As shown on the left and right in Figures 4a and 6a, the short side edges had bowed inward. There were small shear lips located along the long edges. In both Figure 4b and 6b, the fractures exhibited an angled orientation with a two-level morphology. These angled faces are towards the reader in both figures. The fractures in Figures 4a and 4b exhibited a dull, gray luster with a rough surface texture.

Similarly, the fracture surfaces along unriveted arms of the clips also exhibited surface features with a dull, gray luster and rough surface texture. Each of these fractures, located near the corner of the bridge, exhibited a concave orientation (see Figures 3b and 5b), though in opposite directions.

The fracture surfaces were examined as received using a scanning electron microscope (SEM). Figures 7 through 11 highlight selected areas on the A clip fracture surfaces, as the B clip fracture surfaces exhibited comparable features and patterns. Figure 7 shows a typical area of one of the clip fracture surfaces, exhibiting elongated features, consistent with the grain direction from the working of the metal in the clip shape. The tortuous surface morphology is exemplified in Figure 8, with the elongated grain structure angled in the figure from lower left to upper right. A closer view of these features revealed dimpled rupture, consistent with overstress fracture (Figure 9).

Figure 10 shows the initiation of the overstress fracture of the clasp-less arm of the A clip. At a lower magnification, the fracture surface exhibited flow lines and river patterns, consistent with the overstress fracture beginning at the inside corner and advancing outward. At the corner shown in Figure 11, there were no features consistent with pre-existing cracks or other features leading to local stress concentrations. Likewise, the opposite riveted arm of the same clip exhibited flow lines consistent with overstress fracture starting at the inside corner surface (Figure 12). Concurrent with these fracture patterns were parallel tears along the inner surface near the fracture surface.

These features were consistent with overstress fracture of the seat belt clips. The morphology of the fracture surfaces was consistent with tensile overstress fracture of the arms with the riveted clasps, and outward (sideways) bending overstress of the non-riveted arms. There were no features observed indicative of pre-existing cracking.

The composition of the clip was examined using energy dispersive x-ray spectroscopy (EDS) and x-ray fluorescence (XRF). The chemical composition was consistent with a 7000-series aluminum alloy. The hardness was inspected per ASTM E18 and averaged 89 HRBW. [1] The electrical conductivity was inspected per ASTM E1004 and

[1] ASTM E18 – *Standard Test Methods for Rockwell Hardness and Rockwell Superficial Hardness of Metallic Materials*. ASTM International, West Conshohocken, PA.

averaged 33.2% IACS.[2] Based on AMS 2658, these data were consistent with a T6 or peak-aged temper for this class of alloys.[3] This temper is to impart peak hardness and mechanical properties for this class of aluminum alloys.

Erik M Mueller
Materials Research Engineer

[2] ASTM E1004 – *Standard Test Method for Determining Electrical Conductivity Using the Electromagnetic (Eddy-Current) Method.* ASTM International, West Conshohocken, PA
[3] AMS 2658 – *Hardness and Conductivity Inspection of Wrought Aluminum Alloy Parts*. SAE International, Warrendale, PA.

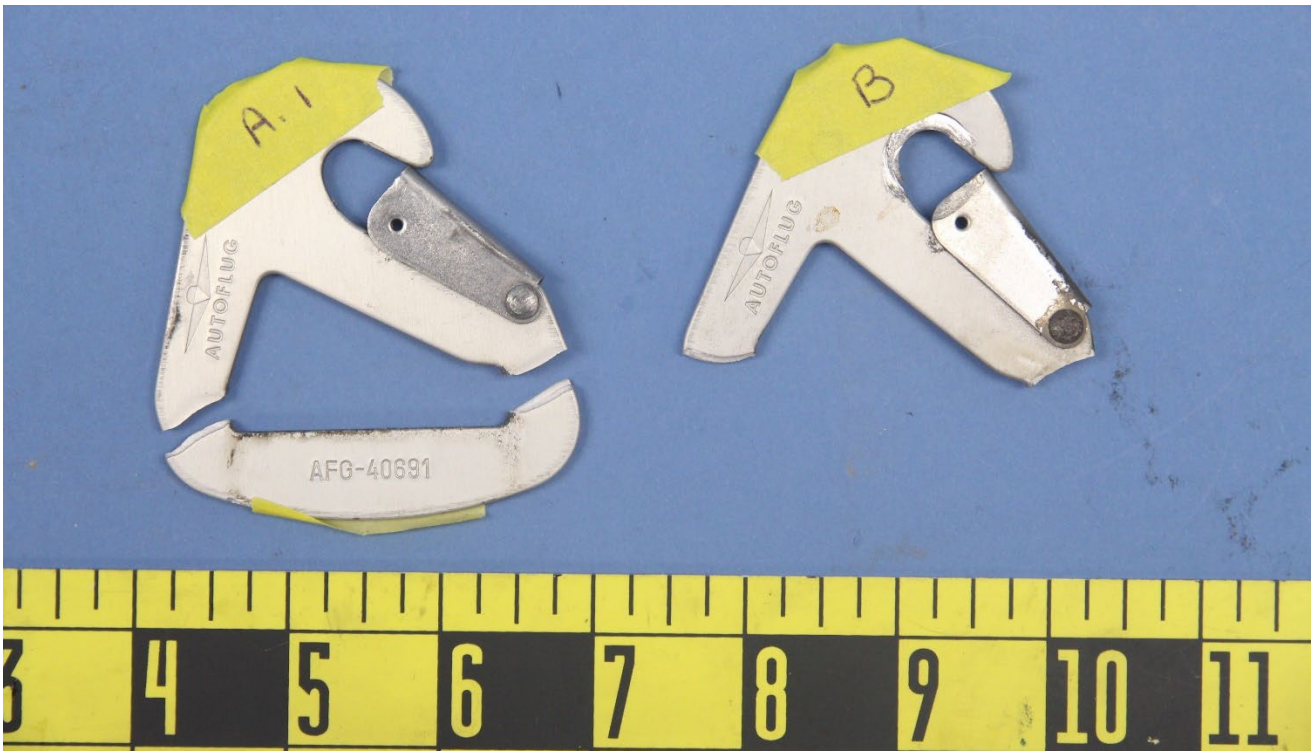

Figure 1 – Views of the seat belt clip remnants, as received, with the A clip on the left and the B clip on the left.

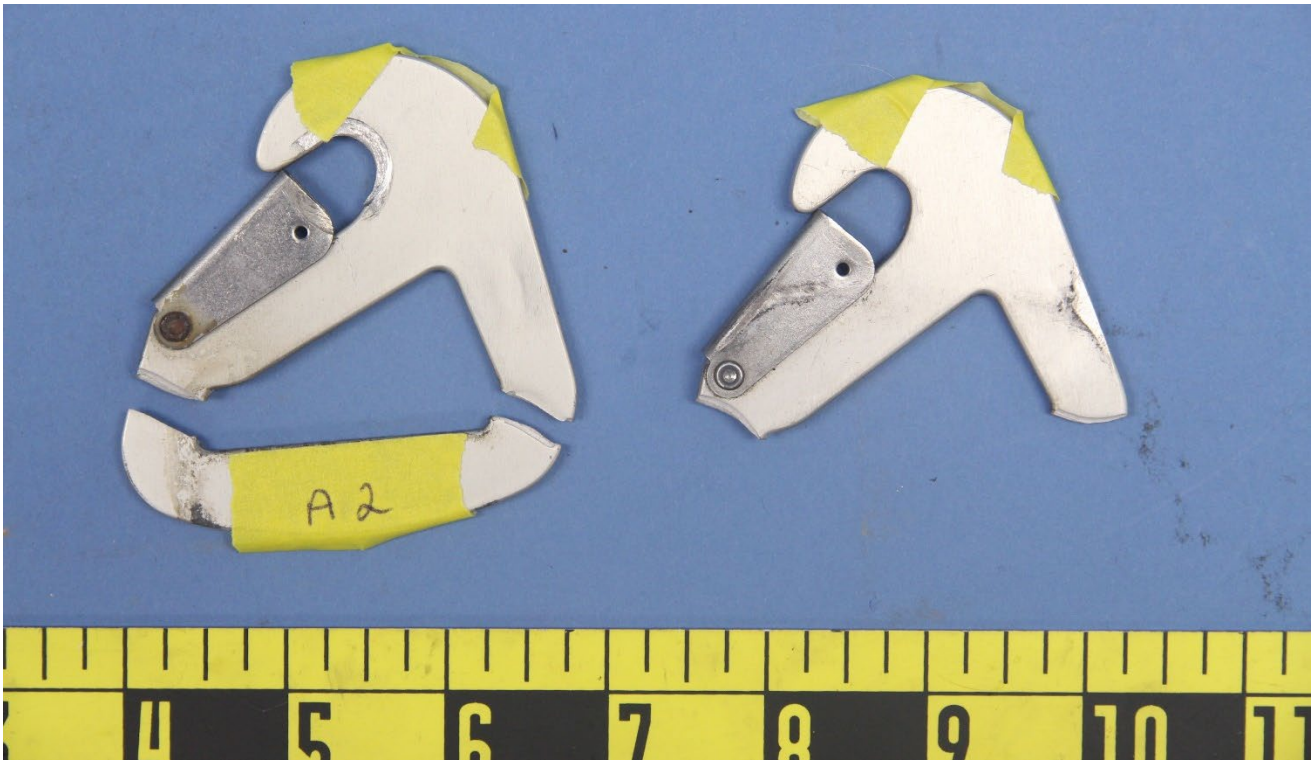

Figure 2 – Reverse views of the seat belt clips from Figure 1.

Figure 3 – View of the B clip fracture surface on the non-riveted arm from (a) the surface and (b) the side, as received.

Figure 4 – View of the B clip fracture surface on the riveted arm from (a) the surface and (b) the side, as received.

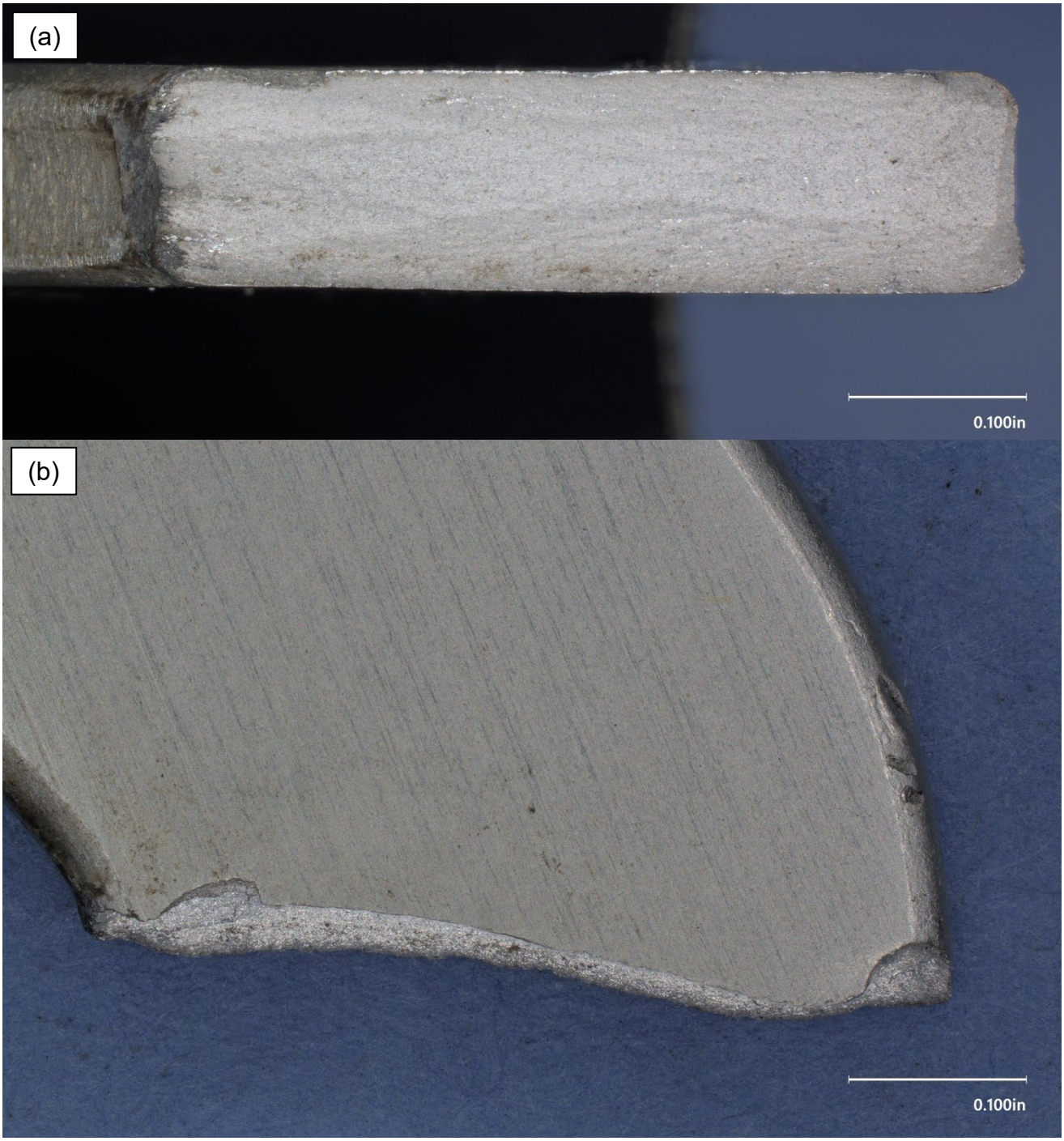

Figure 5 – View of the A clip fracture surface on the non-riveted arm from (a) the surface and (b) the side, as received.

Figure 6 – View of the A clip fracture surface on the riveted arm from (a) the surface and (b) the side, as received.

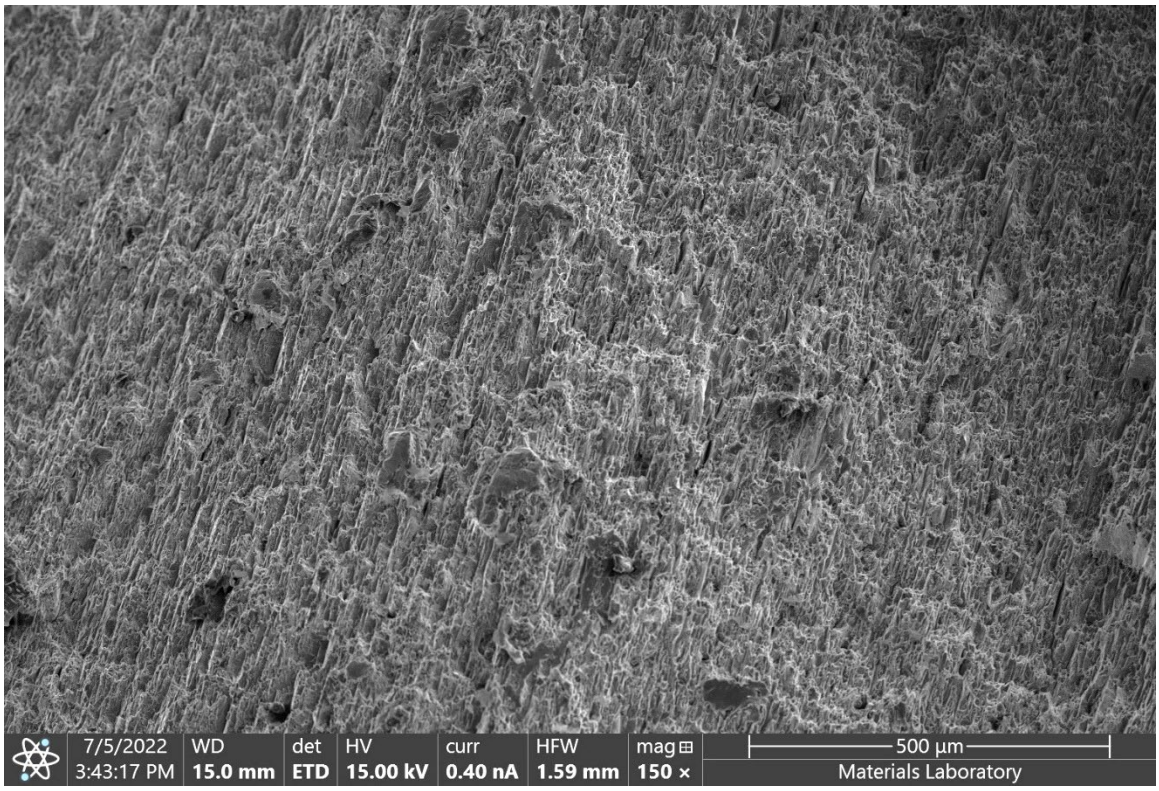

Figure 7 – Secondary electron (SE) micrograph of the fracture surface of the non-riveted arm of the A clip fracture surface.

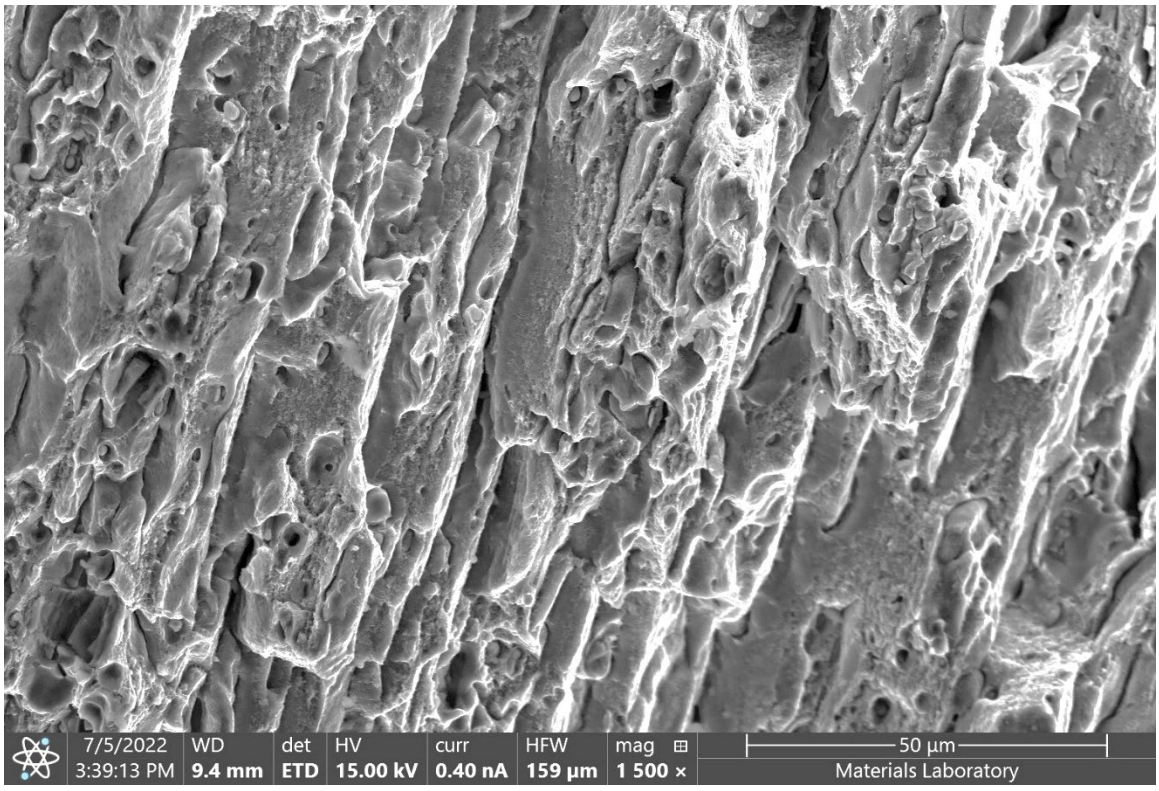

Figure 8 – SE micrograph of a closer view of fracture features in Figure 7.

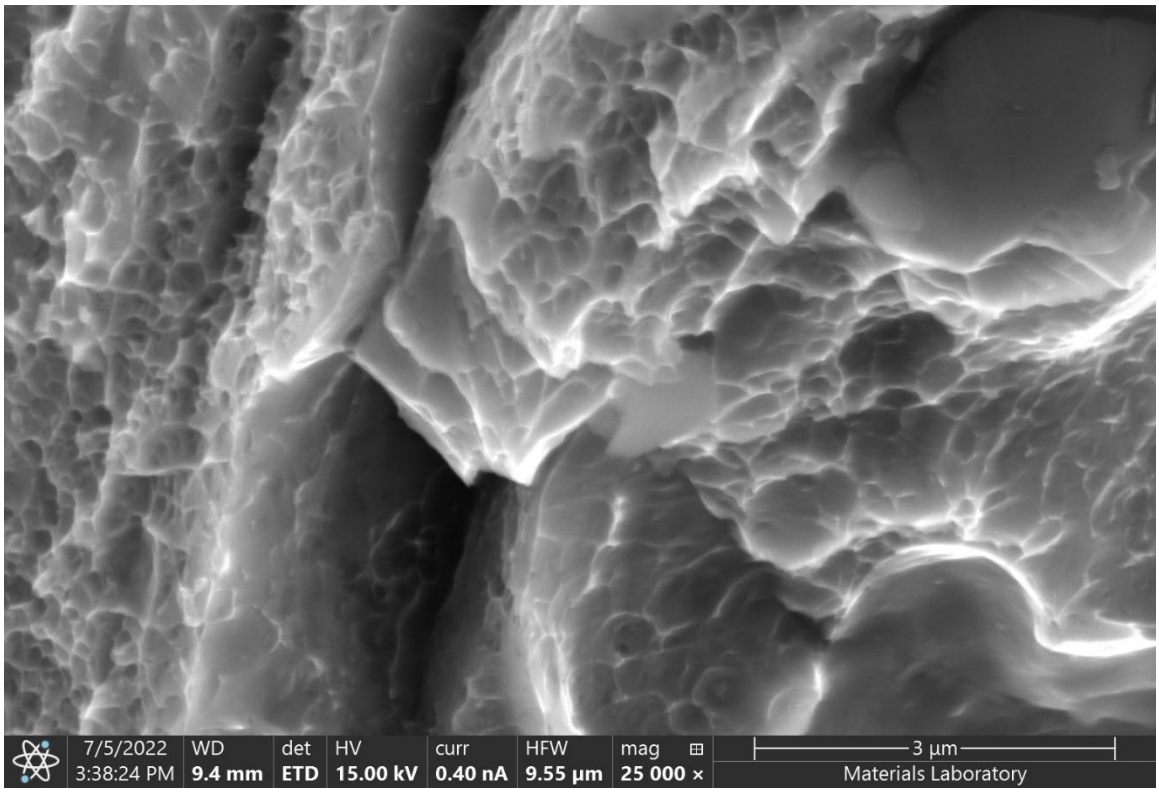

Figure 9 – SE micrograph of fine dimpled rupture in Figure 8.

Figure 10 – SE micrograph of the inside edge of the non-riveted arm of the A clip.

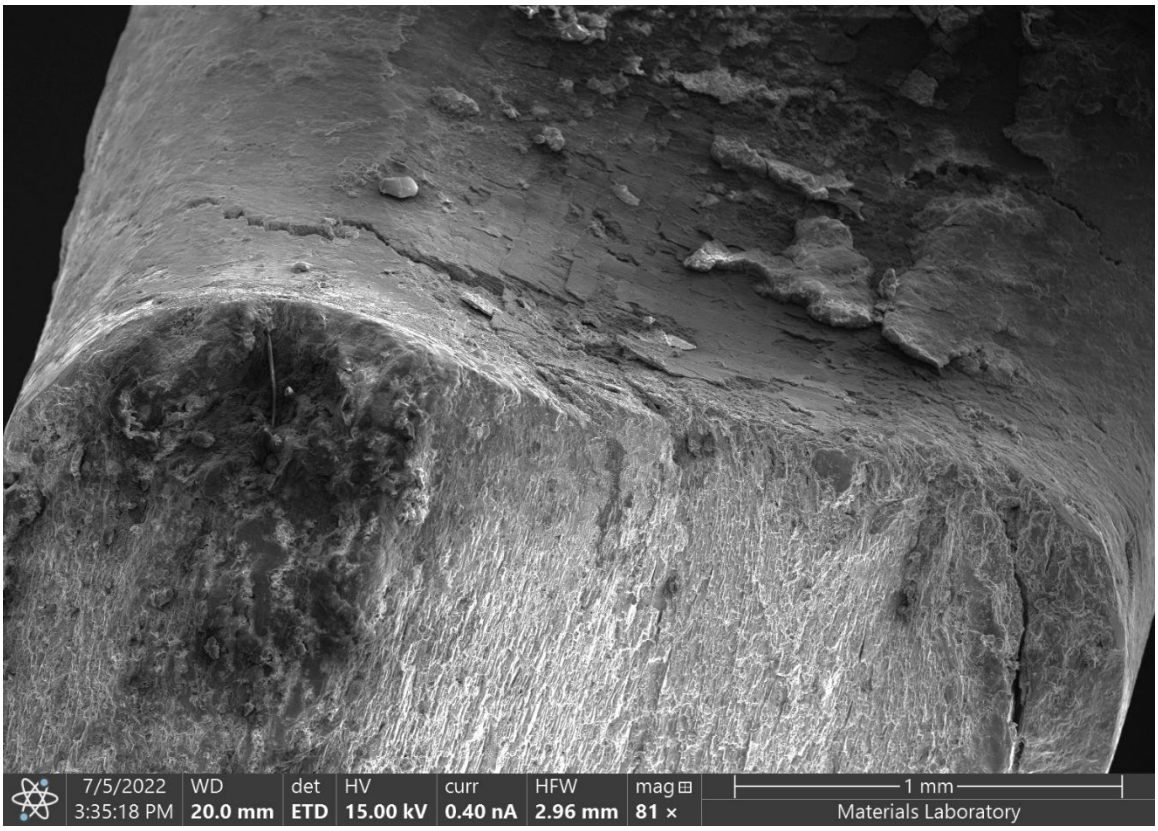

Figure 11 – SE micrograph of the inside corner of the fracture surface of the opposite riveted A-clip arm, showing tearing near and along the fracture.